

Adsorption of Cr(VI) in aqueous solution using sago bark (*Metroxylon sagu*) as a new potential biosorbent

Syiffa Fauzia^a, Hermansyah Aziz^b, Dahyunir Dahlan^c, Jacek Namieśnik^d, Rahmiana Zein^{a,*}

^aLaboratory of Analytical Environmental Chemistry, Department of Chemistry, Andalas University, Padang 25163, West Sumatra, Indonesia, Tel. +62751-71671; Fax: +62751-73118; emails: mimiedison@yahoo.co.id, rzein@sci.unand.ac.id (R. Zein), syiffafauzia@gmail.com (S. Fauzia)

^bLaboratory of Physical Chemistry, Department of Chemistry, Andalas University, Padang, Indonesia, Tel. +62751-71671; Fax: +62751-73118; email: haziz13@yahoo.com

^cLaboratory of Material and Structure, Department of Physics, Andalas University, Padang 25163, Indonesia, Tel. +62 82387463421; Fax: +62751-73118; email: dahyunir@yahoo.com

^dDepartment of Analytical Chemistry, Chemical Faculty, Gdansk University of Technology, 11/12 G Narutowicza, 80-952 Gdansk, Poland, Tel. +48 58 347 10 10; email: jacek.namiesnik@pg.edu.pl

Received 5 June 2018; Accepted 9 December 2018

ABSTRACT

This paper investigated the ability of sago bark (*Metroxylon sagu*) as a new potential biosorbent in removing Cr(VI) in batch system. The optimum adsorption capacity of sago bark (*Metroxylon sagu*) was 61.73 mg/g achieved at pH 3, agitation rate of 100 rpm, contact time 60 min, particle size $\leq 32 \mu\text{m}$, and initial concentration of Cr(VI) 1,000 mg/L at room temperature (25°C). The adsorbent regeneration was carried out using 0.01 M HNO₃ with regeneration efficiency of 78.35%. The adsorption data fitted better to Freundlich and Langmuir equilibrium isotherm models. The data confirmed that Cr(VI) sorption onto sago bark (*Metroxylon sagu*) has good agreement with pseudo-second-order model. The thermodynamic study indicated that Cr(VI) sorption onto sago bark (*Metroxylon sagu*) occurred as exothermic in nature ($\Delta H = -72.55 \text{ kJ/mol}$), which was required energy for adsorption process, and the disorderliness decreased as temperature increased ($\Delta S = -263.06 \text{ J/mol}$). Thus, it can be concluded that sago bark (*Metroxylon sagu*) can be utilized as a potential adsorbent in Cr(VI) removal.

Keywords: Adsorption; Cr(VI); *Metroxylon sagu*; Batch

1. Introduction

Recently, water pollution becomes a significant issue all around the world. Human activities such as industry, restaurant, textile industry, and the electroplating process produce a large amount of waste. The waste has a bad influence on water quality, biodiversity, and extinction of some animals living in the water. Heavy metals were discharged from wastewater into the water bodies. Chromium(VI) is one of the toxic metals produced in an industrial process

[1,2]. Chromium(VI) exists as Cr₂O₇²⁻, CrO₄²⁻, and HCrO₄⁻ ions in solution. It can cause damage to the biological system in the body and is carcinogenic. United States Environmental Protection Agency emphasizes the maximum amount of chromium in wastewater and potable water is 1.0 and 0.05 mg/L, respectively [3]. Numerous methods have been used to treat metal ions in aqueous solution such as chemical precipitation, membrane filtration, electrochemical method, and ion exchange. The efficiency of these methods was not sufficient for large-scale application due to

* Corresponding author.

the high cost and resulting in other compounds as residue [4–6]. Adsorption technique was chosen to treat metal ions because it is more efficient and short-time and low-cost operation. Hence, the metal ion adsorption used an agricultural by-product/waste as an adsorbent to reduce wastewater treatment cost [7]. Adsorption of metal ions has been done using a number of adsorbents such as biochar from paper mulberry [8], lychee peel [9], *Artimisia absinthium* seed [10], coir pith [11], wool [12], *Phaleria macrocarpa* [13], *Dimorcarpus longan* [14], *Garcinia Mangostana* [15], AC from oak leaves and date palm dead leaves [16,17], and other agricultural by-products.

Sago (*Metroxylon sago*) plant is used in sago starch production industries. This industry extracts the starch and produces the residue from sago starch processing. Sago bark is one of the solid residues of sago production industries. The sago industry produces about 5–10 t bark/d. It is usually used as timber fuel, fence, and building materials. Sago bark consists of lignin, and it is associated with hemicelluloses in wall cell of sago pith, non-condensed syringyl unit, non-condensed guaiacyl unit, non-condensed *p*-hydroxyphenyl unit, and cellulose [18,19]. This sago bark is not used effectively yet. Thus, the aim of this research was to investigate the ability of sago bark (*Metroxylon sago*) on removal anion of Cr(VI) adsorption in a batch reactor.

2. Experimental

2.1. Materials

The sago (*Metroxylon sago*) bark was collected from a local area of West Sumatra, Indonesia. The reagents used in this work were potassium dichromate ($K_2Cr_2O_7$), buffer (pH 2–7), sodium hydroxide (NaOH), and nitric acid (HNO_3), which are produced by Merck. All solutions were of analytical grade and prepared in distilled water.

2.2. Adsorbent preparation

The sago bark, collected from local area, was washed to eliminate dirt. Then, sundried for 1 week before ground into particular particle sizes (32, 72, 160, and 425 μm). Later, 1 kg of powder was immersed into HNO_3 0.01 M for 2 h. The powder of sago barks was washed with distilled water until neutral pH was reached. Then, it was dried to remove water in a room temperature.

2.3. Adsorbent characterization

The characterization of adsorbent was carried out by FTIR (Fourier transform infrared, Unicam Mattson Mod 7000 FTIR), SEM-EDX (scanning electron microscopy energy-dispersive X-ray, Hitachi S-3400N), BET (Breuner–Emmet–Teller/Quantachrome Nova 4200e), XRF (X-ray fluorescence spectroscopy/PANalytical epsilon 3), and ICP (inductively coupled plasma/ICPE 9000 Shimadzu, Japan). Point of zero charge (pH_{pzc}) was investigated according to Ahmad et al. [6]. Twenty-five milliliters of KCl 0.1 M with various pH (1–8) was contacted with 0.05 g adsorbent for 24 h at 100 rpm of agitation rate. Then, the final pH (pH_f) of each solution was measured and plotted against initial pH (pH_i).

2.4. Adsorption studies

The batch technique was carried out by adding 0.1 g adsorbent into 10 mL of Cr(VI) solution under certain parameters such as pH 2–7, agitation rate 50–200 rpm, contact time 5–90 min, initial concentration 20–1,400 mg/L, temperature 298–318 K, particle size of adsorbent 32–425 μm , and adsorption-desorption cycle. The concentration of Cr(VI) after adsorption was determined by atomic absorption spectrophotometer (AA240). The amount of Cr(VI) ion adsorbed was determined by the following equation:

$$\text{Adsorption efficiency (\%)} = \frac{C_0 - C_e}{C_0} \times 100 \quad (1)$$

$$\text{Adsorption capacity} \left(\frac{\text{mg}}{\text{g}} \right) = \frac{C_0 - C_e}{m} \times V \quad (2)$$

where C_0 and C_e (mg/L) are initial and the equilibrium concentrations of liquid phase, respectively. V (L) is the volume of Cr(VI) solution and m (g) is the mass of the adsorbent.

3. Results and discussion

3.1. Adsorbent characterization

To identify the functional group involved in adsorption process, FTIR was employed to spot wave number shift of functional group existed in sago bark. The broadband in the region of 3,276–3,500 cm^{-1} indicated the presence of free and intermolecular bonded –OH and –NH groups. The bands at 3,421.10 and 1,734.16 cm^{-1} were hydroxyl (OH) and carbonyl (C=O) groups, respectively. The C–H stretching group was indicated at 2,923.73 cm^{-1} . After adsorption process, the band of each functional groups was shifted. The hydroxyl group band was shifted from 3,421.10 to 3,424.46 cm^{-1} after Cr(VI) uptake. The carbonyl (C=O) and C–H stretching groups were shifted from 1,734.16 to 1,735.49 cm^{-1} and from 2,923.73 to 2,922.42 cm^{-1} , respectively (Fig. 1). This phenomenon was also found by previous researches [20–22]. As the metal ions contacted with adsorbent, the adsorbent composition changed. The XRF data verified that Cr(VI) has attached on sago bark proven by change of chemical composition in adsorbent (Table 1). pH_{pzc} showed that sago bark surface has zero charge at pH 5 (Fig. 3). When $pH < pH_{pzc}$, the adsorbent surface would be positively charged, and at $pH > pH_{pzc}$, the adsorbent surface would be negatively charged [6]. Morphology of sago bark surface was characterized by SEM with 1,000 \times magnification. It could clearly explain that the adsorbent surface which is initially porous and rough became smoother because it was covered by metal ions. The EDX spectra proved that Cr(VI) ion has attached on adsorbent surface (Fig. 2). According to BET analysis, sago bark has 4.845 m^2/g of surface area with distribution pore 24.904 \AA . The total pore volume and average pore diameter are 0.01342 cc/g and 55.39 \AA , respectively. The surface area of sago bark changed after adsorption process from 4.845 to 730.319 m^2/g . This phenomenon indicated that the interaction between metal ion and adsorbent might occur chemically through complex formation, ion exchange, or electrostatic interaction or physically through the pores [23].

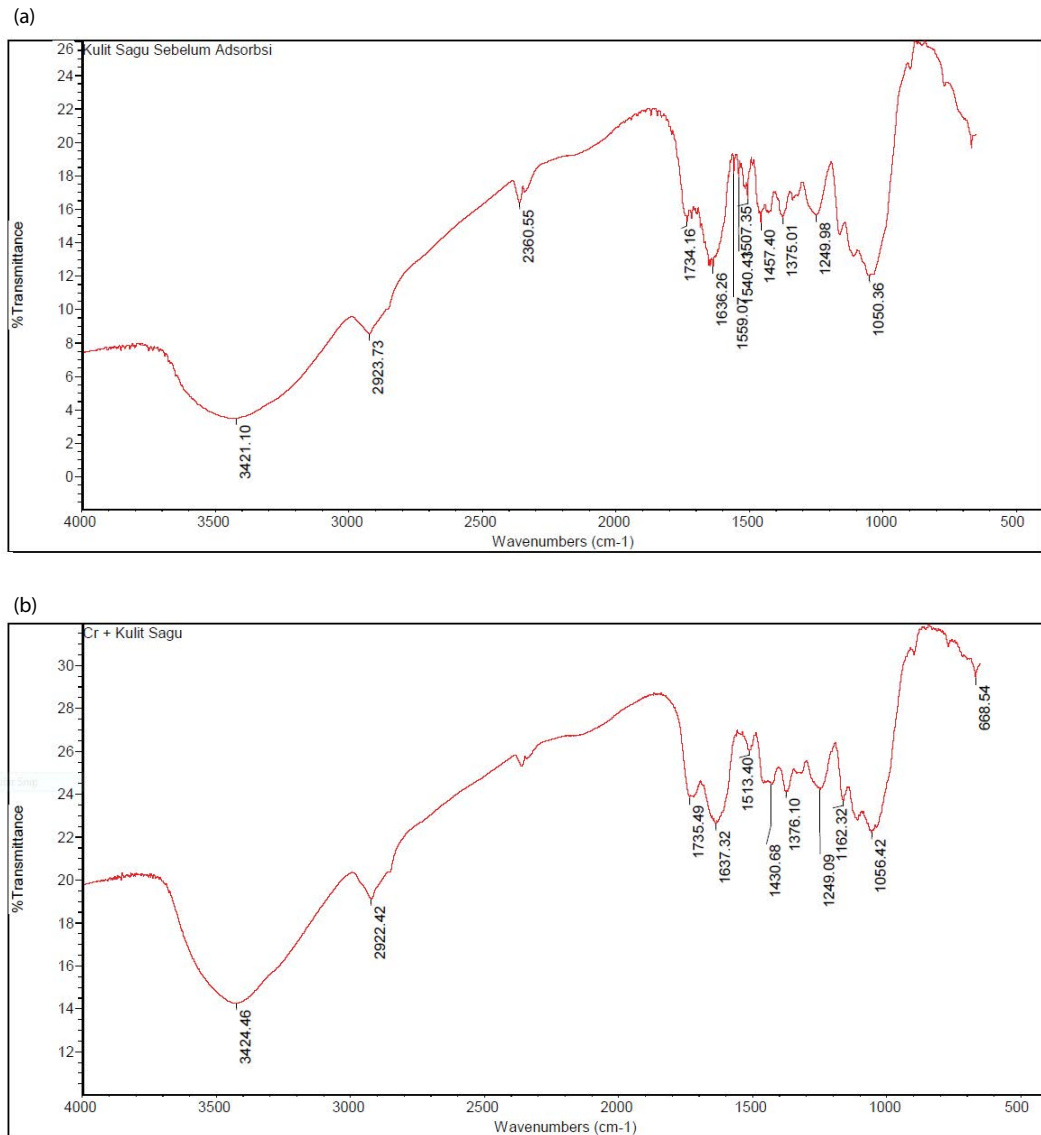


Fig. 1. FTIR spectra of sago bark (a) before adsorption and (b) after Cr(VI) sorption.

Table 1
XRF study of sago bark

Before adsorption		After adsorption	
compound	Concentration (%w/w)	compound	Concentration (%w/w)
Mg	7.74	Mg	8.82
Si	29.84	Si	33.82
Ca	16.10	Ca	16.56
K	7.81	K	2.05
MgO	9.12	MgO	10.16
SiO	39.47	SiO	42.08
CaO	10.84	CaO	10.10
K ₂ O	4.79	K ₂ O	1.13
Cr	0.07	Cr	1.51

3.2. Adsorption study

3.2.1. Effect of pH

pH plays an important role on sorption process. pH affected the surface charge of adsorbent which is related to interaction between adsorbent and metal ions. The effect of pH was studied within the range of 2–7. As seen in Fig. 3, the maximum adsorption capacity was achieved at pH 3. Because at low pH, the adsorbent surface was protonated. The protonated adsorbent surface exhibited the electrostatic force with Cr(VI), which existed in HCrO_4^- , CrO_4^{2-} , and $\text{Cr}_2\text{O}_7^{2-}$ forms [8,19,24,25]. Then, at $\text{pH} > 3$, adsorption capacity decreased from 1.1244 to 0.3468 mg/g due to the huge number of OH^- ions making the adsorbent surface negatively charged. It generated the repulsion force between oxy-anion and adsorbent surface [26,27]. Furthermore, this might attribute to the sago bark pH_{pzc} . pH_{pzc} was the point where the

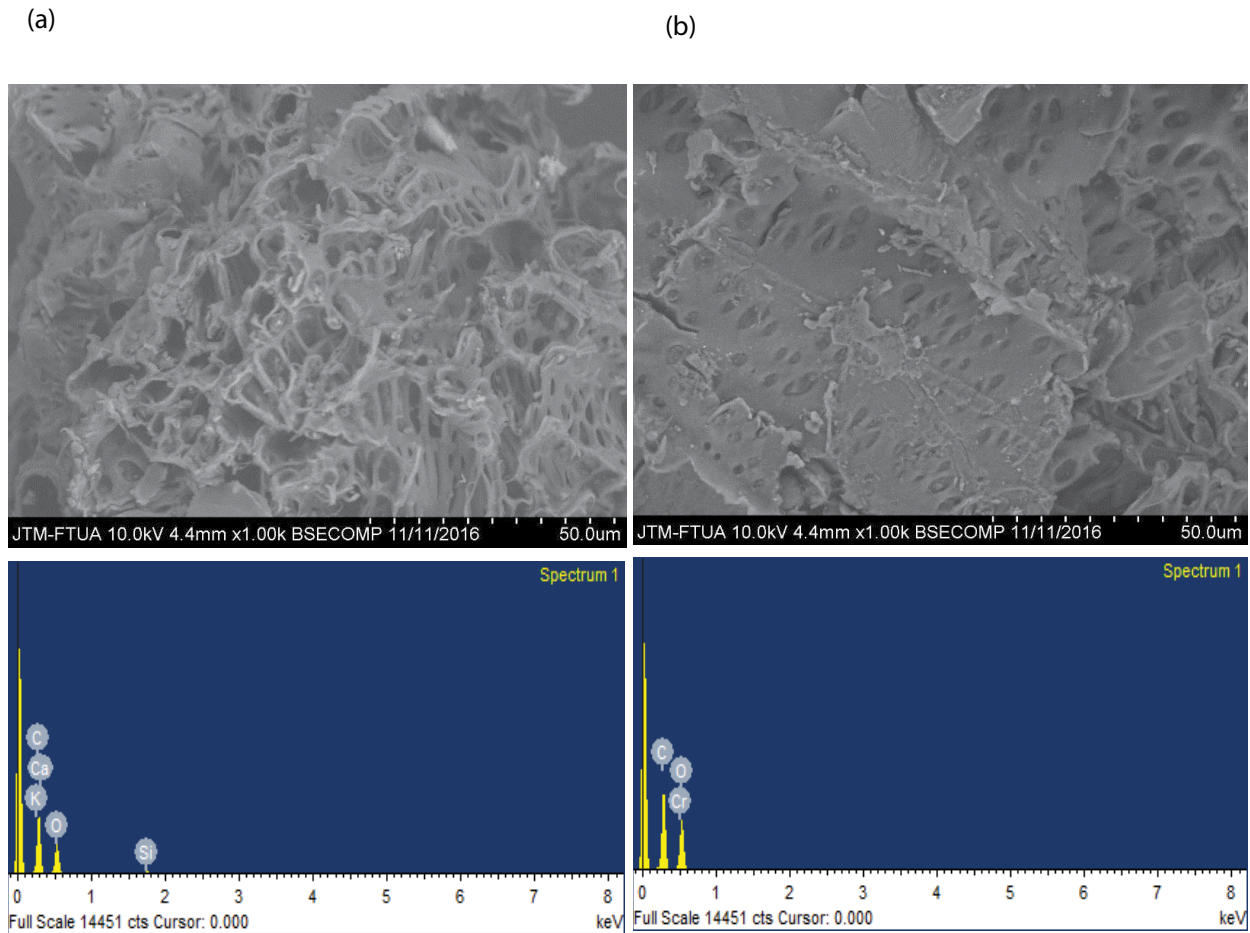


Fig. 2. SEM-EDX image of sago bark (a) before and (b) after Cr(VI) sorption, magnification 1,000×.

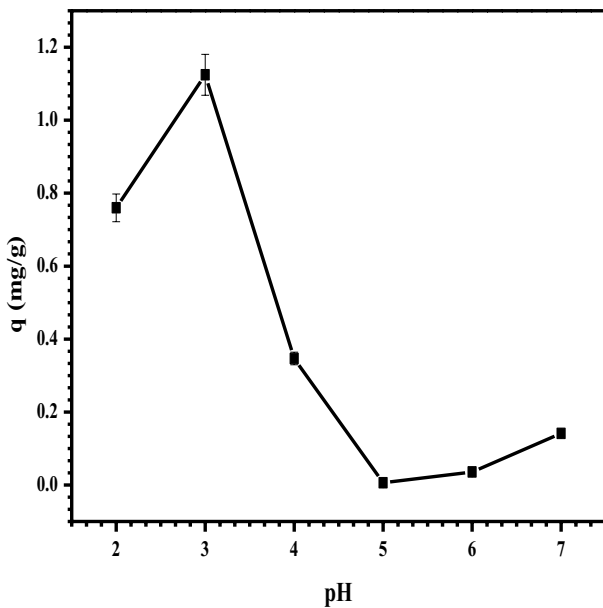


Fig. 3. The effect of pH on the adsorption of Cr(VI) with sago bark (initial concentration at 20 mg/L, contact time in 60 min, agitation rate at 100 rpm, and adsorbent mass was 0.1 g).

adsorbent surface charge has the equal number of positive and negative charges [28]. Fig. 4 exhibits that pH_{zpc} of sago was 5. Above pH_{zpc} adsorbent surface will be negatively charged due to functional group deprotonation establishing anionic-dominated surface and vice versa. The functional group protonation occurred in acidic medium ($pH < pH_{zpc}$) providing positively charged adsorbent surface [6,29,30]. Therefore, Cr(VI) sorption, which existed in negatively charged ions, reached the peak at low pH (pH 3). The similar finding has been reported by previous research [28].

3.2.2. Effect of agitation rate

The agitation influenced the boundary layer around adsorbent. During the adsorption process, this boundary layer will break and allow the metal ions to contact with active site [27,31]. Fig. 5 indicates that the adsorption capacity of sago bark increased as the agitation rate increased until equilibrium was attained. Adsorption of Cr(VI) onto sago bark achieved maximum point at 100 rpm of agitation speed with adsorption capacity 1.7669 mg/g. At the lower speed, adsorbent was accumulated at the bottom of the flask, which declined the adsorption capacity of sago bark. Moreover, the decrease in the adsorption capacity was also induced by

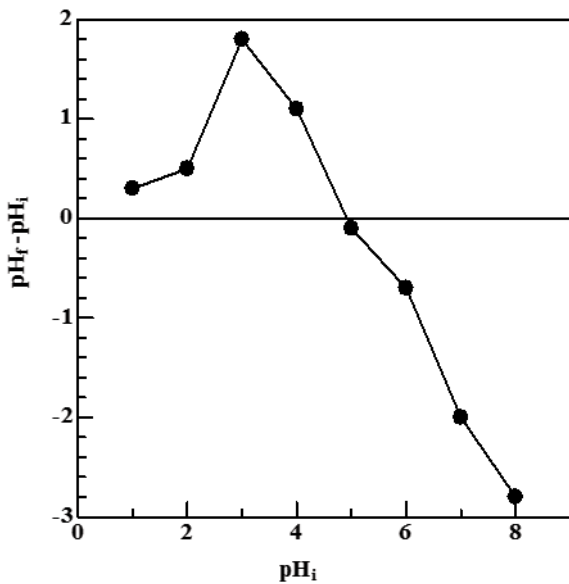


Fig. 4. Point of zero charge determination.

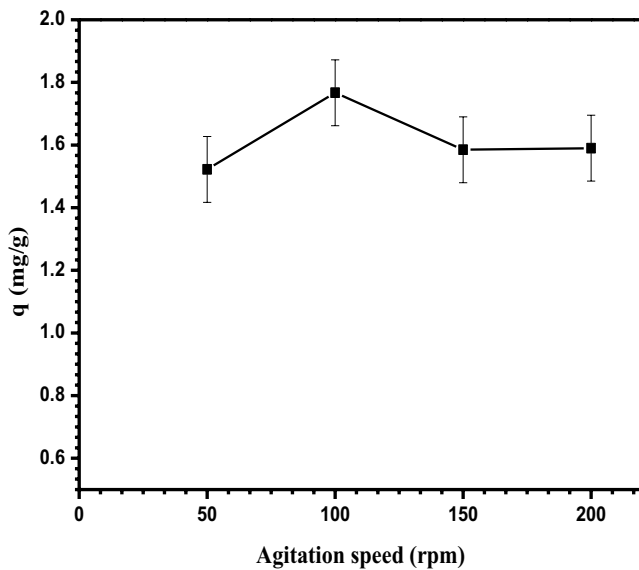


Fig. 5. The effect of agitation rate on the adsorption of Cr(VI) with sago bark (at pH 3, contact time in 60 min, initial concentration was 20 mg/L, and adsorbent mass was 0.1 g).

the higher speed. In this case, when the agitation speed was higher than 100 rpm, the adsorbed metal ions were released to liquid phase due to low affinity toward against active site [32,33]. This phenomenon has been confirmed by previous researches [27,33].

3.2.3. Effect of contact time and kinetic study

Contact time is the time required to reach an equilibrium where the adsorption capacity does not change significantly [24,34]. Contact time shows minimum time for adsorption to take place and also adsorbent surface saturation [3,35].

Fig. 6 reveals an effect of contact time on Cr(IV) sorption. In this case, Cr(VI) sorption attained equilibrium at 60 min with adsorption capacity 1.7669 mg/g and then gradually decreased as the time increased. This phenomenon could be explained by the vacant surface of adsorbent at initial phase leading to easy adsorption of metal ions onto active site [2]. Adsorption reaction mechanism of Cr(VI) on sago bark was explained by pseudo-first order, pseudo-second order, and Webber-Morris intraparticle diffusion. In the pseudo-first order, the linear plot was achieved by using the following equation [36,37]:

$$\log(q_e - q_t) = \log q_e - \frac{k_1 t}{2.303} \quad (3)$$

where q_e is the adsorption capacity at equilibrium (mg/g), q_t is the adsorption capacity at t (mg/g), k_1 is the rate constant (min^{-1}) from the slope, and t is time (min).

Pseudo-second order was described by the following equation [36,37]:

$$\frac{t}{q_t} = \frac{1}{k_2 q_e^2} + \frac{t}{q_e} \quad (4)$$

where k_2 is the rate constant of pseudo-second order ($\text{g}/\text{mg}\cdot\text{min}$).

The intraparticle diffusion was utilized to explained the diffusion mechanism. This model was expressed by following equation [26,29,38]:

$$q_t = k_{id} \sqrt{t} + C \quad (5)$$

where k_{id} and C were intraparticle diffusion rate constant ($\text{mg}/\text{g}\ \text{min}^{1/2}$) and intercept.

The adsorption capacities at equilibrium from pseudo-first-order and pseudo-second-order models were calculated

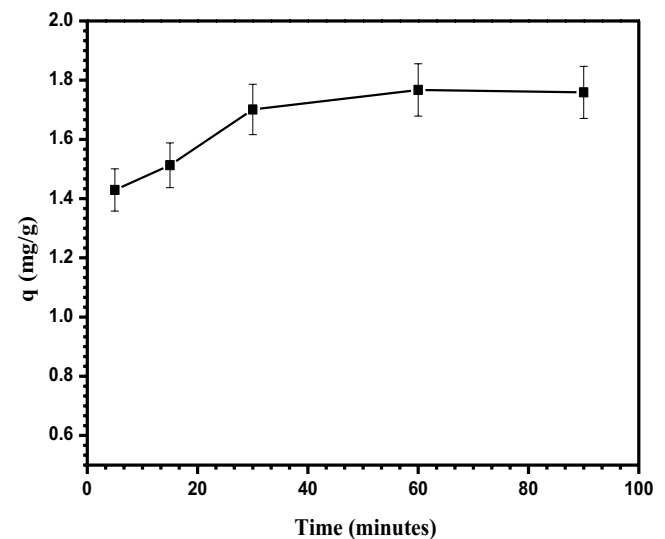


Fig. 6. The effect of contact time on the adsorption of Cr(VI) with sago bark (at pH 3, agitation rate at 100 rpm, initial concentration was 20 mg/L, and adsorbent mass was 0.1 g).

as 0.3818 and 1.8021 mg/g for the initial Cr(VI) concentration of 20 mg/L, respectively (Table 2). The experimental q_e value (1.7669 mg/g) was close to calculated q_e value from pseudo-second-order model. The Webber-Morris model indicated that adsorption of Cr(VI) onto sago bark can be explained by two mechanisms. The first stage, from 5 to

30 min, attributed to macropore diffusion/external surface adsorption. The second stage, from 30 to 90 min, exhibited intraparticle diffusion adsorption (Fig. 7). The intraparticle rate constant (k_{id}) was 0.049 mg/g min^{1/2} and C (intercept) was 1.3512 showing the existence of boundary layer effect (Table 2). The determination coefficient indicated that

Table 2
The kinetic parameters of Cr(VI)

Pseudo-first order			Pseudo-second order			Webber-Morris intraparticle diffusion		
k_1 (min ⁻¹)	q_e (mg/g)	R^2	k_2 (g/mg·min)	q_e (mg/g)	R^2	k_{id} (mg/g·min ^{1/2})	C	R^2
0.0437	0.3818	0.9673	0.2956	1.8021	0.9996	0.049	1.3512	0.9283

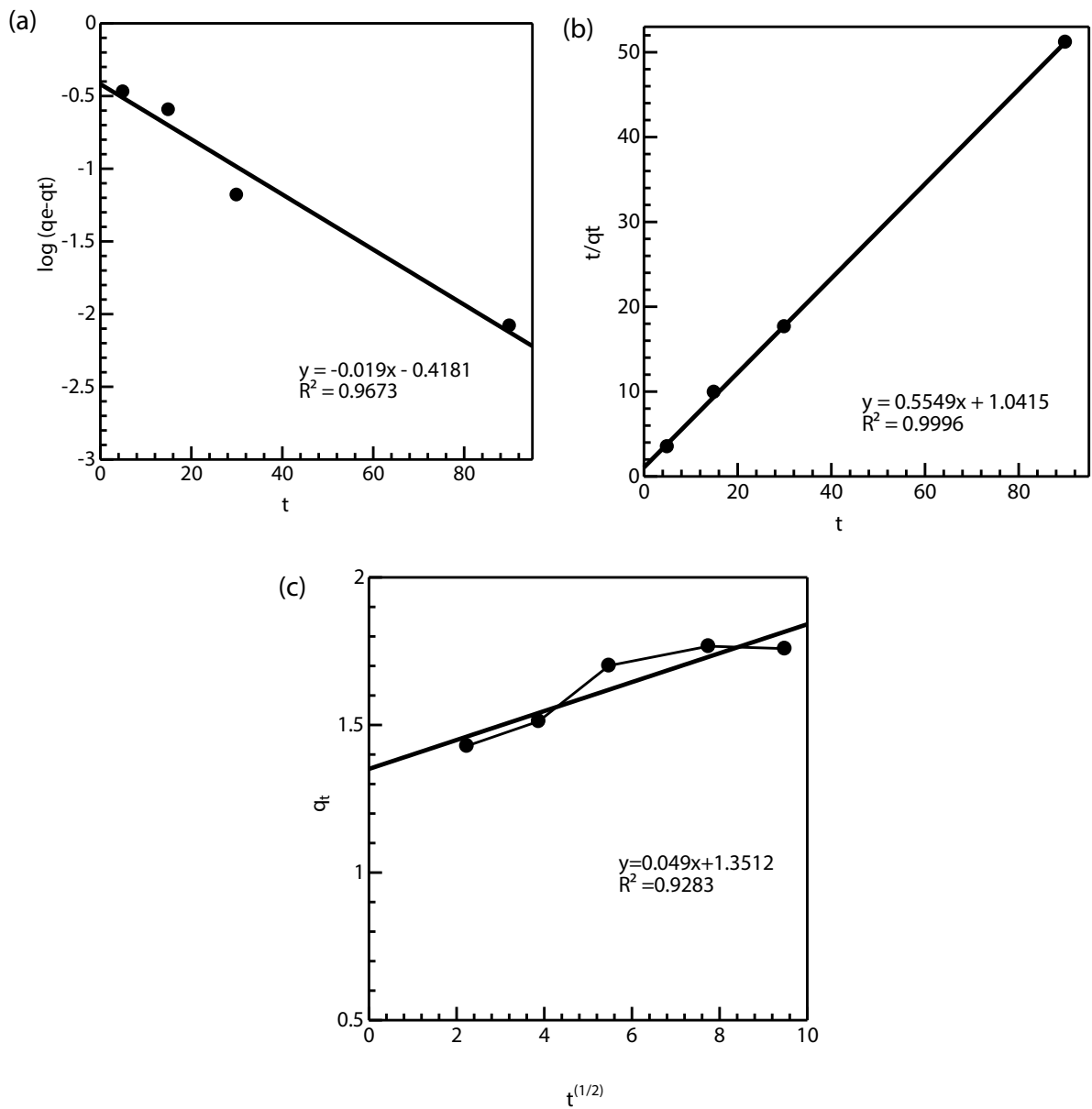


Fig. 7. Adsorption kinetics of Cr(VI) onto sago bark: (a) pseudo-first order, (b) Pseudo-second order, and (c) Webber-Morris intraparticle diffusion.

pseudo-second order ($R^2 = 0.9996$) fitted well to describe Cr(VI) sorption reaction (Table 2). Also, the experimental q_e value (1.7669 mg/g) was close to calculated q_e value from pseudo-second-order model. This result suggested that the Cr(VI) sorption onto sago bark was controlled by chemisorption reaction through exchanging or sharing electron [36,37] and intraparticle diffusion rate-limiting step [26,29,38].

3.2.4. Effect of particle size

Effect of particle size of sago bark powder was studied in various sizes of 32–425 μm . Fig. 8 shows that as particle size increased, the adsorption capacity decreased due to the surface area decrease. The smaller particle size had the more active site available for the adsorption process [2], and the smaller particle facilitated metal ion to diffuse onto adsorbent easily [38,39]. The adsorption capacity of sago bark decreased from 47.38 to 27.74 mg/g as particle size increased from 32 to 425 μm . Therefore, 32 μm of particle size was preferred for further use.

3.2.5. Effect of initial concentration and equilibrium study

Fig. 9 indicates the Cr(VI) ion initial concentration effect in the range of 20–1,400 mg/L. As seen in Fig. 7, the adsorption capacity decreased as the concentration increased. At the initial stage, adsorption occurred faster due to the vacant surface availability of the exchangeable site. But as concentration increased, metal ion uptake became slower because the active sites have been occupied by metal ions causing a competition to occupy the active site which led to the reduction of metal uptake [1,3,24]. Cr(VI) attained the peak at concentration of 1,000 mg/L with adsorption capacity of 61.73 mg/g.

Equilibrium adsorption of Cr(VI) onto sago bark was studied by Langmuir, Freundlich, and Temkin equilibrium

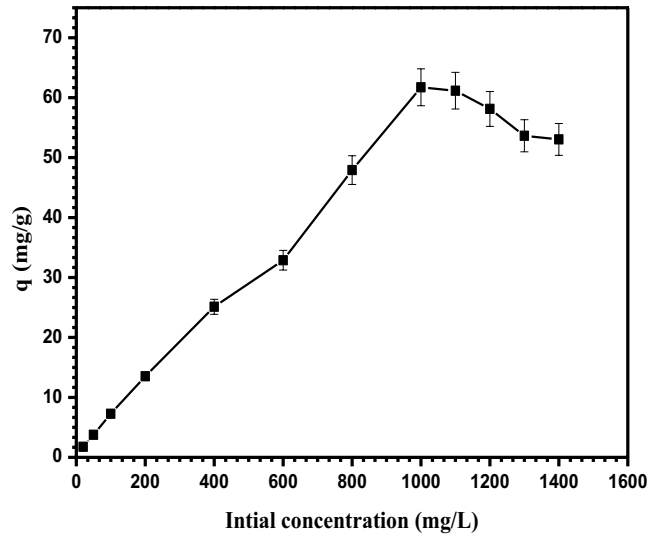


Fig. 9. The effect of initial concentration on the adsorption of Cr(VI) with sago bark (at pH 3, agitation rate at 100 rpm, contact time in 60 min, and adsorbent mass 0.1 g).

isotherm models. Langmuir equilibrium isotherm model is expressed by the equation below:

$$\frac{C_e}{q_e} = \frac{1}{Q_{\max} \times K_L} + \frac{C_e}{Q_{\max}} \quad (6)$$

The curve was conducted by plotting C_e/q_e vs. C_e , where C_e is the equilibrium concentration of the adsorbate (mg/L), q_e is the adsorption capacity at equilibrium (mg/g), Q_{\max} is the maximum adsorption capacity (mg/g), and K_L is the Langmuir equilibrium constant (L/mg). Langmuir isotherm is based on assumptions that adsorption is limited to monolayer coverage, the active sites are similar and only able to bind one atom of adsorbate, and the ability of the molecule to adsorb onto active sites is independent of its neighborhood [40,41].

Whereas Freundlich equilibrium isotherm model was described by the following equation:

$$\ln q_e = \ln K_F + \frac{1}{n} \ln C_e \quad (7)$$

Linear plots were obtained by plotting $\ln q_e$ vs $\ln C_e$. Where q_e is adsorption capacity (mg/g), K_F is Freundlich constant (L/mg), and $1/n$ is Freundlich adsorption intensity parameter. Freundlich has favorable adsorption constant n , between 1 and 10 ($0.1 < 1/n < 1$ means favorability of adsorption). This isotherm has an assumption that the active sites are distributed exponentially with respect to the heat of adsorption [40,41]. The equation and the linearized form of Temkin equilibrium isotherm model were represented as follows (plotting q_e vs $\ln C_e$):

$$q_e = \frac{RT}{b} \ln K_T + \frac{RT}{b} \ln C_e \quad (8)$$

where b is the Temkin constant related to the heat of adsorption (J/mol), K_T Temkin constant (L/g), R is the gas

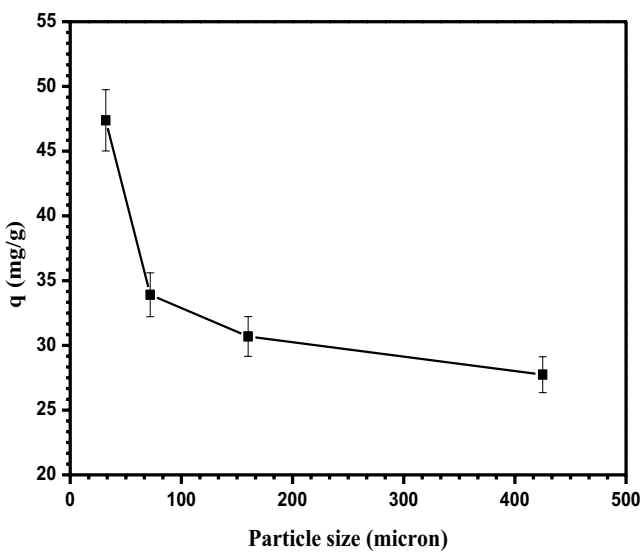


Fig. 8. The effect of particle size on the adsorption of Cr(VI) with sago bark (at pH 3, agitation rate at 100 rpm, contact time in 60 min, initial concentration 1,000 mg/L, and adsorbent mass 0.1 g).

constant (8.314 J/mol·K), and T is absolute temperature (K) [30]. Fig. 8 was linear plots of Langmuir, Freundlich, and Temkin equilibrium isotherm models. As listed in Table 3, the Langmuir model indicated that q_{\max} was 70.9219 mg/g. The Temkin model described the heat of adsorption represented by b . The experiment exhibited exothermic sorption process due to $b > 0$ ($b = 213.768$ J/mol) [30]. It was also confirmed by the negative enthalpy (thermodynamic parameters). Meanwhile, the Freundlich model showed n parameter, which obeyed an order if $n = 1$, adsorption

was linear; $n < 1$, chemisorption occurrence; and $n > 1$, physical sorption occurrences. The experimental result revealed physical sorption reaction between sago bark and Cr(VI) due to $n = 1.5501$ ($n > 1$). Based on the determination coefficient (R^2), Cr(VI) sorption onto sago bark fitted to Freundlich and Langmuir equilibrium isotherm models, which assumed the chemical sorption through strong electrostatic interaction, ion exchange, or complex formation [40,41] and physical sorption through pore interaction (Fig. 10).

Table 3
The adsorption model parameters on Cr(VI) sorption

Langmuir			Freundlich			Temkin		
q_{\max} (mg/g)	K_L (L/mg)	R^2	K_F (L/mg)	n	R^2	b (J/mol)	K_T (L/mg)	R^2
70.9219	0.00503	0.919	0.9261	1.5501	0.9757	213.768	0.1466	0.8316

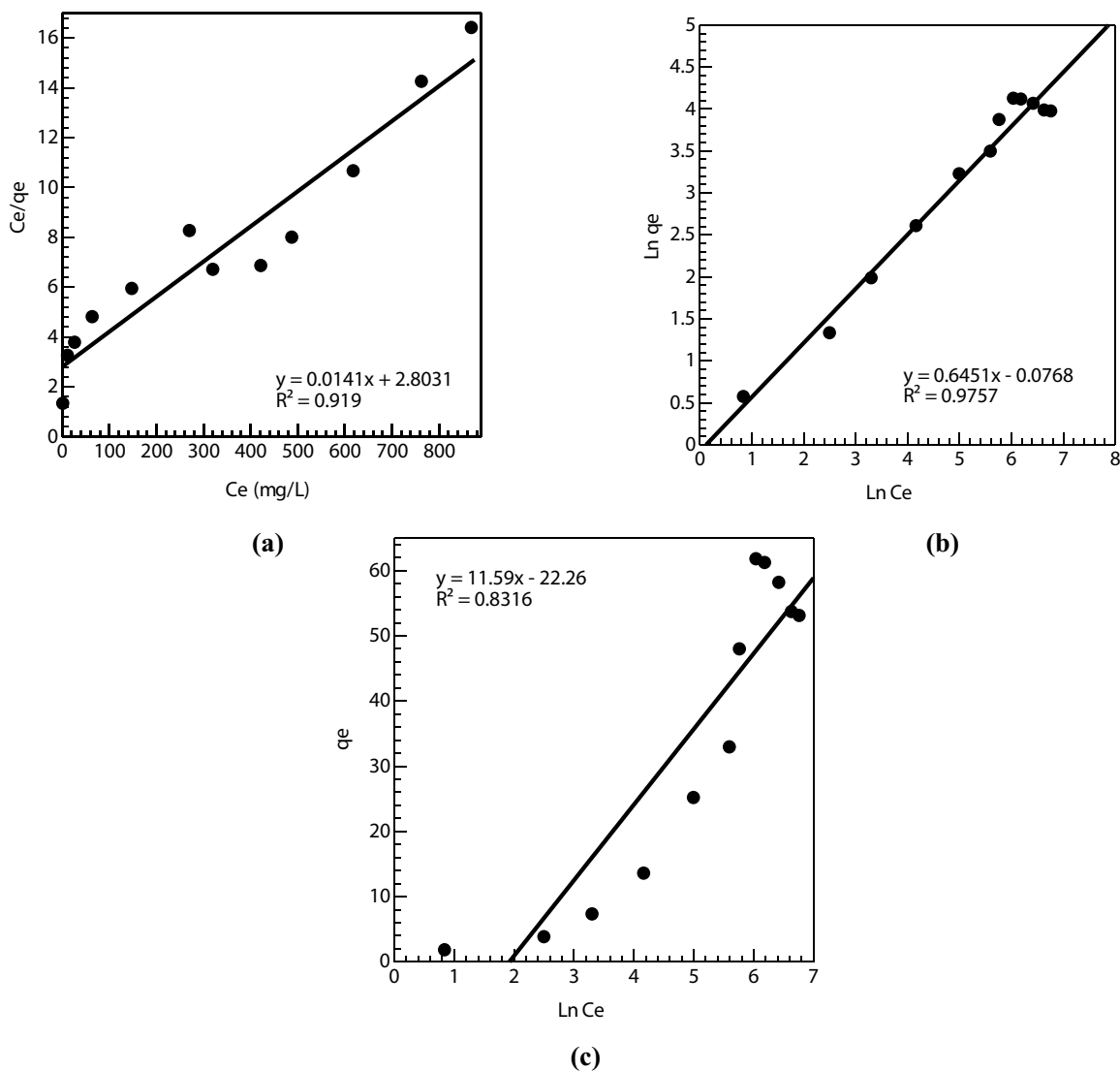


Fig. 10. Isotherm plots for Cr(IV) adsorption onto sago bark: (a) Langmuir, (b) Freundlich, and (c) Temkin.

3.2.6. Thermodynamic evaluation

The effect of temperature was studied at 298, 308, and 318 K with varying concentrations in the range of 10–50 mg/L, contact time 60 min, adsorbent dose 0.1 g, and agitation rate 100 rpm. Fig. 11 reveals as temperature increased, adsorption capacity of sago bark increased. At temperature 298 K, the adsorption capacity of sago bark was 3.4685 mg/L (initial concentration at 50 mg/L); as temperature increased, the adsorption capacity slightly decreased to 3.035 mg/L at temperature 318 K. This result indicated the exothermic process on adsorption process of Cr(VI) with sago bark. This result was confirmed by thermodynamic parameters derived from Van't Hoff equation:

$$\Delta G^\circ = -RT \ln KI \quad (9)$$

$$\ln KI = \frac{\Delta S}{R} - \frac{\Delta H}{RT} \quad (10)$$

$$\Delta G^\circ = \Delta H^\circ - T\Delta S^\circ \quad (11)$$

where KI is the equilibrium constant related to the Langmuir constant K_L , R is the gas constant (8.314 J/mol·K), and T is the absolute temperature (K). The thermodynamic parameters were calculated by plotting $\ln KI$ Vs $\frac{1}{T}$. The enthalpy and entropy were defined from slope and intercept of the linear plot.

Table 4 indicates the enthalpy, entropy, and free-energy gibs of Cr(VI) sorption with sago bark. The enthalpy (ΔH°) and entropy (ΔS°) of Cr(VI) sorption were -72.55 kJ/mol and -263.06 J/mol·K, respectively. It revealed exothermic reaction and decreased in disorder of Cr(VI) sorption with sago bark, whereas ΔG° shows a positive value which increased as temperature increased. This led to unspontaneous reaction that required energy for adsorption process. The same result had been reported by other literatures [2,35].

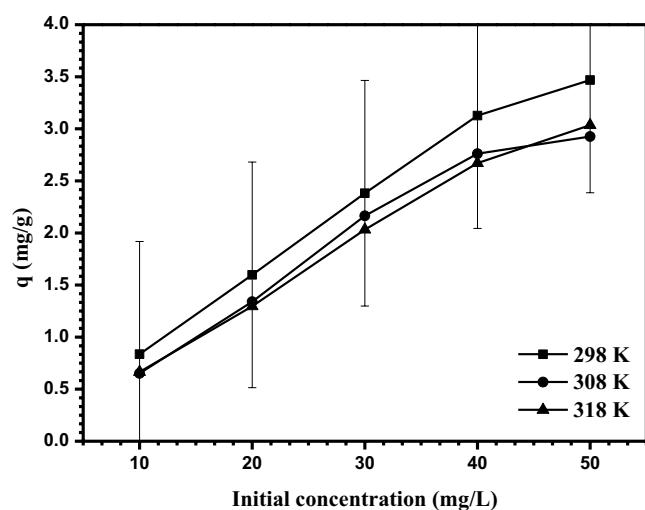


Fig. 11. The effect of temperature on the adsorption of Cr(VI) with sago bark (at pH 3, agitation rate at 100 rpm, contact time 60 min, and adsorbent mass 0.1 g).

Table 4
The thermodynamic parameters on Cr(VI) sorption

T (K)	ΔG° (kJ/mol)	ΔH° (kJ/mol)	ΔS° (J/mol·K)
298	5.83	-72.55	-263.06
308	8.46		
318	11.09		

3.2.7. Adsorption-desorption cycle

The adsorbent regeneration is important in the industrial process due to determining wastewater treatment cost. The adsorption study was conducted by adding 0.1 g adsorbent to 10 mL Cr(VI) solution of 20 mg/L and agitated for an hour at 100 rpm. Then, the desorption study was examined using 10 mL of HNO_3 at varying concentrations (0.1 and 0.01 M) as a desorbing agent, and it was shaken at 100 rpm of agitation rate for an hour [26]. It can be observed from Fig. 12 that adsorption capacity of sago bark decreased after 3 adsorption-desorption Cr(VI) cycles. The adsorption capacity declined from 0.2786 to 0.1504 mg/g after the third cycle having desorption efficiency 81.42% with HNO_3 0.1M as desorbing agent. Meanwhile, HNO_3 0.01 M caused a decrease in adsorption capacity from 0.2786 to 0.1880 mg/g after 3 adsorption-desorption cycles with desorption efficiency of 78.35%. The result showed that desorbing agent concentration affected the adsorbent capability on metal ion removal. HNO_3 0.01M performed good result compared with HNO_3 0.1M because the adsorption capacity did not change significantly between the second and the third cycle. This condition occurred due to the functional group breakdown in higher acidic medium when it was used time after time. Nevertheless, there was no significant difference in Cr(VI) sorption after 2 adsorption-desorption cycles. Thus, it could be interpreted that sago bark has promising adsorption capacity and reproducibility. Adsorption capacities of some other adsorbents were presented in Table 5.

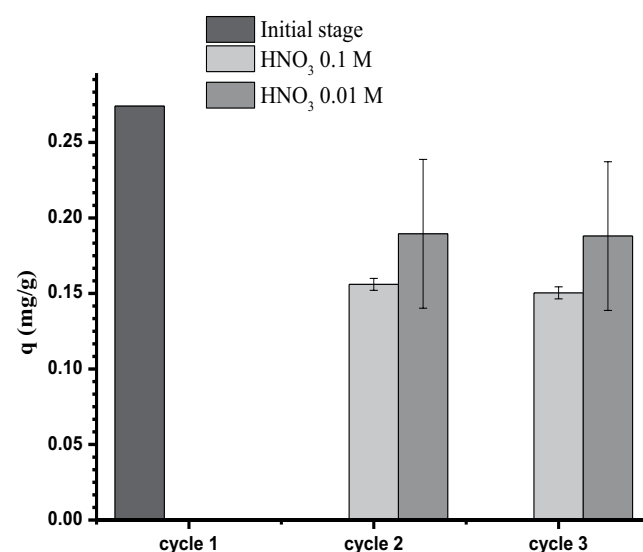


Fig. 12. Adsorption capacity of sago bark after 3 adsorption-desorption Cr(VI) cycles.

Table 5
Previous research on Cr(VI) removal by some adsorbents

Adsorbent	Q (mg/g)	Reference
Granular activated carbon	0.99	[43]
citrate-coated magnetite nanoparticles (NPs)	4.65	[44]
Peanut hull	6.53	[24]
Peanut hull	14.13	[39]
Ash gourd	18.7	[28]
Raw rutin	26.3	[26]
Rutin resin	41.3	
<i>Acacia nilotica</i>	39.21	[1]
Sago bark	61.73	Present study

3.2.8. Adsorption mechanism

The adsorption mechanism of Cr(VI) removal on sago bark could be explained by adsorbent characteristic and experimental data resulted in experiment. There are several mechanisms suggested on Cr(VI) sorption such as electrostatic interaction, reduction, ion exchange, complexation, and adsorption through the pores [23]. The pH_{zpc} of sago bark was 5 indicating that at pH lower than 5 the sago bark surface would be positively charged. Since, the optimum pH on Cr(VI) sorption was reached at pH 3, it meant that electrostatic interaction existed between adsorbent and Cr(VI) ion because at $pH < 6$ Cr(VI) dominant species was $Cr_2O_7^{2-}$ and $HCrO_4^-$. These data were also supported by kinetic and isotherm models. Pseudo-second-order and Webber-Morris kinetic models were found appropriate to describe the mechanism of Cr(VI) sorption onto sago bark. These models proposed that adsorption process was chemical rate-limiting step and intraparticle rate-limiting step through sharing or exchanging electron. The Webber-Morris model described that the adsorption process experienced the external diffusion at the initial stage so that adsorption happened faster. Later, when the surface has been covered, the adsorption process was carried out through internal diffusion. But it became slower. Thus, the adsorption capacity did not significantly change (Fig. 7(c)) [19,29,36–38]. These data were also confirmed by isotherm model that followed Langmuir and Freundlich isotherm models, pointing that physical and chemical sorptions (electrostatic interaction, ion exchange, or complex formation) occur as adsorption mechanism on Cr(VI) removal [40,41]. The adsorbent characteristic was shown by wave shift in FTIR spectra. The hydroxyl group band was shifted from 3,421.10 to 3,424.46 cm^{-1} . The carbonyl and C–H stretching groups were shifted from 1,734.16 to 1,735.49 cm^{-1} and from 2,923.73 cm^{-1} to 2,922.42 cm^{-1} , respectively. Although the wave number was not significantly shifted, this indicated the change in vibrational energy of the functional group. This phenomenon was also found by previous research [20–22]. The wave number shift of oxygen-containing functional group and C–H stretching group was concerned in the reduction of Cr(VI) to Cr(III). The Cr(III) could exchange with K, Mg, or Ca ion and establish complexation with other functional group [23] (Fig. 13). This is proved by XRF, pointing that concentration change of these cations in the solid phase

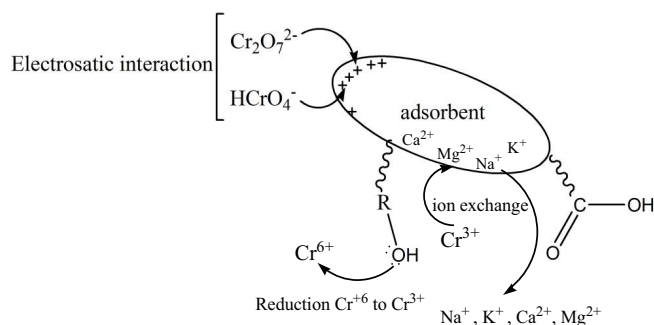


Fig. 13. Cr(VI) sorption mechanism onto sago bark.

Table 6
Concentration of cation released in liquid phase

Cation released in the liquid phase (mg/L)			
Na^+	K^+	Ca^{2+}	Mg^{2+}
1.22	8.62	0.966	0.0862

(Table 1) and ICP revealed these ion existence in the liquid phase (Table 6). The BET analysis indicated that the average pore diameter of sago bark was 55.39 Å with distribution pore 24.904 Å. These facts gave the possibility toward Cr(VI) to fill and trap into the pore of sago bark since the hydrated radius of Cr(VI) was 4.61 Å. The SEM image showed the surface alteration after the adsorption process occurred. The porous surface of sago bark was covered by Cr(VI) ion that was proven by the appearance of Cr(VI) spectra at EDX image (Fig. 2). This confirmed that physical adsorption has taken place on Cr(VI) sorption onto sago bark. Therefore, the Cr(VI) mechanism onto sago bark involved both physical and chemical reactions [42].

4. Conclusions

Sago bark (*Metroxylon sago*) has an ability to remove Cr(VI) ion in solution as a low-cost adsorbent with adsorption capacity of 61.73 mg/g with no significant reduction after three adsorption-desorption cycles. Thus, it could be concluded that sago bark is a promising adsorbent to treat wastewater containing Cr(VI) ion compared with commercial activated carbon.

Acknowledgement

This work was supported by Ministry of Research Technology and Higher Education of the Republic Indonesia No. grant: 324/SP2H/LT/DPRM/IX/2016 and September 5th, 2016, and Department of Analytical Chemistry, Faculty of Chemistry, Gdansk University of Technology, Poland.

References

- [1] P. Thilagavathy, T. Santhi, *Acacia nilotica* as a low-cost sorbent for the removal of toxic Cr(VI) from single and multicomponent systems using batch and column method: equilibrium isotherm, kinetics and thermodynamic studies, *Int. J. Latest Res. Sci. Technol.*, 3 (2014) 115–122.

- [2] O.R. Adhiambo, K.J. Lusweti, G. Zachary, Biosorption of Pb²⁺ and Cr²⁺ using *Moringa oleifera* and their adsorption isotherms, *Sci. J. Anal. Chem.*, 3 (2015) 100–108.
- [3] S. Ahmad, A. Ali, A. Ashfaq, Removal of Cr(VI) from aqueous metal solution using roasted china clay, *Int. J. Curr. Microbiol. Appl. Sci.*, 5 (2016) 171–185.
- [4] F. Ouadjenia-Marouf, R. Marouf, J. Schott, A. Yahiaoui, Removal of Cu(II), Cd(II) and Cr(III) ions from aqueous solution by dam silt, *Arabian J. Chem.*, 6 (2013) 401–406.
- [5] M.A. Laskar, S.K. Ali, S. Siddiqui, The potential of coriandrum Sativum L. seeds in the remediation of waste water, *Int. J. Adv. Sci. Technol.*, 86 (2016) 41–50.
- [6] R. Ahmad, R. Kumar, S. Haseeb, Adsorption of Cu²⁺ from aqueous solution onto iron oxide coated eggshell powder: evaluation of equilibrium, isotherms, kinetics, and regeneration capacity, *Arabian J. Chem.*, 5 (2012) 353–359.
- [7] F. Fadzil, S. Ibrahim, M. Ahmad, K. Megat, Adsorption of lead (II) onto organic acid modified rubber leaf powder: batch and column studies, *Process Saf. Environ. Prot.*, 100 (2016) 1–8.
- [8] S. Adil, A. Mashiatullah, M. Asma, A. Ghaffar, S. Khan, J. Abid, Adsorption of heavy metals by bio-chars produced from pyrolysis of paper mulberry from simulated industrial wastewater, *Nucleus*, 51 (2014) 323–327.
- [9] R. Ali, K. Rao, F. Rehman, M. Kashifuddin, Removal Cr(VI) from electroplating wastewater using fruit peel of leechi (*Litchi chinensis*), *Desal. Water Treat.*, 49 (2012) 136–146.
- [10] R. Ali, K. Rao, S. Ikram, M.K. Uddin, Removal of Cr(VI) from aqueous solution on seeds of *Artimisia absinthium* (novel plant material), *Desal. Water Treat.*, 54 (2015) 3358–3371.
- [11] B.M.W.P.K. Amarasinghe, Lead and cadmium removal from aqueous medium using coir pith as adsorbent : batch and fixed bed column studies, *J. Trop. For. Environ.*, 1 (2011) 36–47.
- [12] N. Balkaya, N. Bektas, Chromium (VI) sorption from dilute aqueous solutions using wool, *Desal. Water Treat.*, 3 (2009) 43–49.
- [13] A.N. Nasution, Y. Amrina, R. Zein, H. Aziz, E. Munaf, Characteristics of Cd (II) ions using herbal plant of mahkota dewa (*Phaleria macrocarpa*), *J. Chem. Pharm. Res.*, 7 (2015) 189–196.
- [14] R. Ikhtiar, H. Aziz, R. Zein, The removal of Cr (VI) with *Dimocarpus longan* as a low cost biosorbent, *J. Chem. Pharm. Res.*, 7 (2015) 81–88.
- [15] R. Zein, R. Suhaili, F. Earnestly, Indrawaty, E. Munaf, Removal of Pb(II), Cd(II) and Co(II) from aqueous solution using *Garcinia mangostana* L. fruit shell, *J. Hazard. Mater.*, 181 (2010) 52–56.
- [16] M. Sulyman, J. Namiesnik, A. Gierak, Utilization of new activated carbon derived from oak leaves for removal of crystal violet from aqueous solution, *Pol. J. Environ. Stud.*, 23 (2014) 2223–2232.
- [17] M. Sulyman, J. Namiesnik, A. Gierak, Adsorptive Removal of aqueous phase crystal violet dye by low-cost activated carbon obtained from date Palm (L.) dead leaflets, *Eng. Prot. Environ.*, 19 (2016) 611–631.
- [18] D.S. Awg-adeni, S. Abd-Aziz, K. Bujang, M.A. Hassan, Bioconversion of sago residue into value added products, *Afr. J. Biotechnol.*, 9 (2016) 2016–2021.
- [19] O. Ogunsile, A. Anomo, Adsorption of chromium(VI) and cadmium (II) from aqueous solution by soda lignin obtained from nypa palm leaves (*Nypafruitcans*), *Ozean J. Appl. Sci.*, 7 (2014) 43–56.
- [20] M.R. Lasheen, N.S. Ammar, H.S. Ibrahim, Adsorption/desorption of Cd(II), Cu(II) and Pb(II) using chemically modified orange peel: equilibrium and kinetic studies, *Solid State Sci.*, 14 (2012) 202–210.
- [21] O.H. Tukki, J.T. Barminas, S.A. Osemeahon, J.C. Onwuka, R.A. Donatus, Adsorption of colloidal particles of *Moringa oleifera* seeds on clay for water treatment applications, *J. Water Supply Res. Technol.*, 65 (2016) 75–86.
- [22] L.Y. Lee, D.Z.B. Chin, X.J. Lee, N. Chemmangattuvalappil, S. Gan, Evaluation of *Abelmoschus esculentus* (lady's finger) seed as a novel biosorbent for the removal of Acid Blue 113 dye from aqueous solutions, *Process Saf. Environ. Prot.*, 94 (2015) 329–338.
- [23] H. Li, X. Dong, B. Evandro, L.M. De Oliveira, Y. Chen, L.Q. Ma, Mechanisms of metal sorption by biochars: Biochar characteristics and modifications, *Chemosphere*, 178 (2017) 466–478.
- [24] S. Sharma, S.D. Maind, S.A. Bhalerao, Studies on Cr(VI) biosorption using cost effective biosorbent: peanut hulls (*Arachis hypogaea* Linn), *Asian J. Sci. Technol.*, 6 (2015) 1425–1435.
- [25] A. Ali, K. Saeed, F. Mabood, Removal of chromium (VI) from aqueous medium using chemically modified banana peels as efficient low-cost adsorbent, *Alexandria Eng. J.*, 55 (2016) 2933–2942.
- [26] N.A. Fathy, S.T. El-Wakeel, R.R. Abd El-Latif, Biosorption and desorption studies on chromium(VI) by novel biosorbents of raw rutin and rutin resin, *J. Environ. Chem. Eng.*, 3 (2015) 1137–1145.
- [27] N.J. Hamadi, A.A. Mohammed, A.H. Ali, Removal of Pb²⁺, Cu²⁺ and Cd²⁺ metals from simulated wastewater in single and competitive system using locally porcelanite, *Int. J. Eng. Sci. Res. Technol.*, 3 (2014) 245–257.
- [28] K.M. Sreenivas, M.B. Inarkar, S.V. Gokhale, S.S. Lele, Re-utilization of ash gourd (*Benincasa hispida*) peel waste for chromium (VI) biosorption: equilibrium and column studies, *J. Environ. Chem. Eng.*, 2 (2014) 455–462.
- [29] E. Cheraghi, E. Ameri, A. Moheb, Adsorption of cadmium ions from aqueous solutions using sesame as a low-cost biosorbent: kinetics and equilibrium studies, *Int. J. Environ. Sci. Technol.*, 12 (2015) 2579–2592.
- [30] S.L. Chan, Y.P. Tan, A.H. Abdullah, S.T. Ong, Equilibrium, kinetic and thermodynamic studies of a new potential biosorbent for the removal of Basic Blue 3 and Congo Red dyes: Pineapple (*Ananas comosus*) plant stem, *J. Taiwan Inst. Chem. Eng.*, 61 (2016) 306–315.
- [31] G.Z. Kyzas, N.K. Lazaridis, A.C. Mitropoulos, Removal of dyes from aqueous solutions with untreated coffee residues as potential low-cost adsorbents: Equilibrium, reuse and thermodynamic approach, *Chem. Eng. J.*, 189–190 (2012) 148–159.
- [32] M. Kanyal, A.A. Bhatt, Removal of heavy metals from water (Cu and Pb) using household waste as an adsorbent, *J. Bioremediat. Biodegrad.*, 6 (2015) 1–6.
- [33] B. Kumar, K. Smita, E. Sánchez, C. Stael, L. Cumbal, Andean *Sacha inchi* (*Plukenetia volubilis* L.) shell biomass as new biosorbents for Pb²⁺ and Cu²⁺ ions, *Ecol. Eng.*, 93 (2016) 152–158.
- [34] J.N. Jadav, S.D. Maind, S.A. Bhalerao, Competitive biosorption of lead(II) ions from aqueous solutions onto *Terminalia catappa* L. leaves as a cost effective biosorbent, *Octa J. Environ. Res.*, 3 (2015) 67–79.
- [35] B.O. Evbuomwan, M.M. Atuka, Kinetics and thermodynamic studies of biosorption of cadmium(II) from aqueous solution onto garden grass (GAG), *J. Chem. Mater. Res.*, 1 (2014) 12–22.
- [36] N.A. Reddy, R. Lakshmi pathy, N.C. Sarada, Application of *Citrullus lanatus* rind as biosorbent for removal of trivalent chromium from aqueous solution, *Alexandria Eng. J.*, 53 (2014) 969–975.
- [37] R. Gill, Q. Nadeem, R. Nadeem, R. Nazir, S. Nawaz, J. Bio, E. Sci, Biosorption capacity of vegetable waste biomass for adsorption of lead and chromium, *J. Biodivers. Environ. Sci.*, 5 (2014) 306–317.
- [38] K.G. Akpomie, F.A. Dawodu, K.O. Adebowale, Mechanism on the sorption of heavy metals from binary-solution by a low cost montmorillonite and its desorption potential, *Alexandria Eng. J.*, 54 (2015) 757–767.
- [39] R.M. Ali, H.A. Hamad, M.M. Hussein, G.F. Malash, Potential of using green adsorbent of heavy metal removal from aqueous solutions: adsorption kinetics, isotherm, thermodynamic, mechanism and economic analysis, *Ecol. Eng.*, 91 (2016) 317–332.
- [40] A. Rotimi, G. Okeoghene, Sorption and Desorption Studies on Toxic Metals From Brewery Effluent Using Eggshell as Adsorbent, *Adv. Nat. Sci.*, 7 (2014) 15–24.

- [41] M. Kumar, R. Tamilarasan, Kinetics, equilibrium data and modeling studies for the sorption of chromium by *Prosopis juliflora* bark carbon, *Arabian J. Chem.*, 10 (2017) S1567–S1577.
- [42] M. Sulyman, J. Namiesnik, A. Gierak, Low-cost adsorbents derived from agricultural by-products/wastes for enhancing contaminant uptakes from wastewater: a review, *Pol. J. Environ. Stud.*, 26 (2017) 479–510.
- [43] H. Choi, J. Cho, K. Baek, J. Yang, J. Lee, Influence of cationic surfactant on adsorption of Cr(VI) onto activated carbon, *J. Hazard. Mater.*, 161 (2009) 1565–1568.
- [44] M.J. Silvia-silvia, O.F. Mijangos-Ricardez, V. Vazquez-Hipolito, S. Matinez-Vargas, J. Lopez-Luna, Single and mixed adsorption of Cd (II) and Cr (VI) onto citrate-coated magnetite nanoparticles, *Desal. Wat. Treat.*, 57 (2016) 4008–4017.